Dephasing-Induced Vibronic Resonances in Difference Frequency Generation Spectroscopy

Ravindra Venkatramani

Department of Physics and Astronomy, University of Rochester, Rochester, New York 14627 and Department of Chemistry, University of California, Irvine, California 92697-2025

Shaul Mukamel*

Department of Chemistry, University of California, Irvine, California 92697-2025

Received: November 22, 2004; In Final Form: January 19, 2005

The difference frequency generation (DFG) signal from a two electronic level system with vibrational modes coupled to a Brownian oscillator bath is computed. Interference effects between two Liouville space pathways result in pure-dephasing-induced, excited-state resonances provided the two excitation pulses overlap and time ordering is not enforced. Numerical simulations of two-dimensional DFG signals illustrate how the ground and excited electronic state resonances may be distinguished.

I. Introduction

Difference frequency generation (DFG) and sum frequency generation (SFG) are coherent, three-wave-mixing techniques wherein two input fields with wavevectors $\mathbf{k}_1$ and $\mathbf{k}_2$ create a third signal field with the combination wavevector $\mathbf{k}_s = \mathbf{k}_1 \pm \mathbf{k}_2$. For centrosymmetric media with inversion symmetry the second-order response vanishes in the dipole approximation,[1,2] making these techniques a versatile tool for the study of oriented crystals or surfaces and interfaces.[3−7] Many frequency-domain[5,6] and time-resolved[8−11] applications have been made. SFG techniques have been applied to study molecular conformations at surfaces and interfaces, liquid interfaces, surface reactions, catalysis, chirality of molecules on thin films, and chiral molecules in solution.[5,12−15] Classical MD simulations were carried out for SFG from liquid/vapor interfaces of water[16,17] and acetone.[18] DFG has further found applications in semiconductors.[10,11]

In this paper we focus on an ultrafast DFG technique known as coherence emission spectroscopy/optical rectification,[19,20] whereby two femtosecond visible pulses resonant with an electronic transition create vibrational coherences in both the ground and the excited electronic states. The generated heterodyne detected infrared field (both amplitude and phase) reveals vibrational modes strongly coupled to the photoexcitation. This technique has been applied using 11 fs pulses to study protein vibrational motions coupled to an electronically excited cofactor in photoactivable single crystals (The photodissociation of the heme cofactor in ordered crystals of myoglobin[19] and the retinal trans → cis photoisomerization in oriented films for bacteriorhodopsin[20]). These experiments have opened up new possibilities for probing protein structure and for following concerted motions induced by an external femtosecond trigger. The signal is calculated for a two electronic level system whose vibrational modes are coupled to an overdamped Brownian oscillator bath[21] with an arbitrary time scale. We further show how the ground and the excited state vibrations may be distinguished by a two-dimensional DFG (TDDFG). Two-dimensional SFG was recently demonstrated for a doubly resonant infrared−visible technique[22] and was shown to be sensitive to the vibrational modes as well as their displacements on the electronic excited state. In our case, 2D frequency−frequency plots from cw experiments show clear signatures of the bath time scale. Interference between different Liouville space pathways leads to excited state resonances which are induced by pure homogeneous-dephasing and therefore vanish in the slow bath limit where the line broadening is strictly inhomogeneous. Similar dephasing-induced resonances (DIR) were observed more than two decades ago in third order, coherent Raman spectroscopies (CRS) for atoms in the gas phase[23] and molecular crystals.[24,25] It has been recognized[26] that DIR carry information about the effect of the electronic dephasing rates on vibrational dynamics. Such resonances were recently observed in DOVE (doubly vibrationally enhanced) four wave mixing experiments on mixtures of acetonitrile, deuterionitrile and deuteriobenzene.[27] Since these resonances have pronounced spectral signatures, they can be used to probe vibrational dynamics following electronic excitation. We show that excited-state DFG resonances have long tails $\propto\hat{\Gamma}/\omega_{vib}$, whereas the ground-state resonances vary as $1/\omega_{vib}$, where $\hat{\Gamma}$ denotes the pure dephasing rate and $1/\omega_{vib}$ denotes a vibrational resonance. Impulsive experiments with well-separated pulses do not show these interferences.[21] However, a combination of two impulsive signals can reproduce the frequency-domain interference. In section II, we calculate the second-order nonlinear response of a multilevel system coupled to a harmonic bath. In section III, we present the double sided Feynman diagrams and expressions for the DFG signals from a two electronic level/vibronic system. We then consider various cases of pulse durations corresponding to pure frequency-domain (cw) (section IV), time-domain (impulsive) (section V), and finite pulse experiments (section VI). Closed expressions are derived for the signal in the limiting cases of fast and slow baths for both cw and impulsive experiments.

II. Second-Order Response of a Multilevel System Coupled To a Gaussian Bath

The second-order polarization is related to the external fields through the second-order response function $S^{(2)}(t_2, t_1)$

$$P^{(2)}(\boldsymbol{r}, t) = \int_0^\infty \mathrm{d}t_2 \int_0^\infty \mathrm{d}t_2\, \mathrm{d}t_1\, E(\boldsymbol{r}, t - t_2)E(\boldsymbol{r}, t - t_2 - t_1)S^{(2)}(t_2, t_1) \quad (1)$$

* To whom correspondence should be addressed.

10.1021/jp0446682 CCC: $30.25
Published on Web 04/06/2005

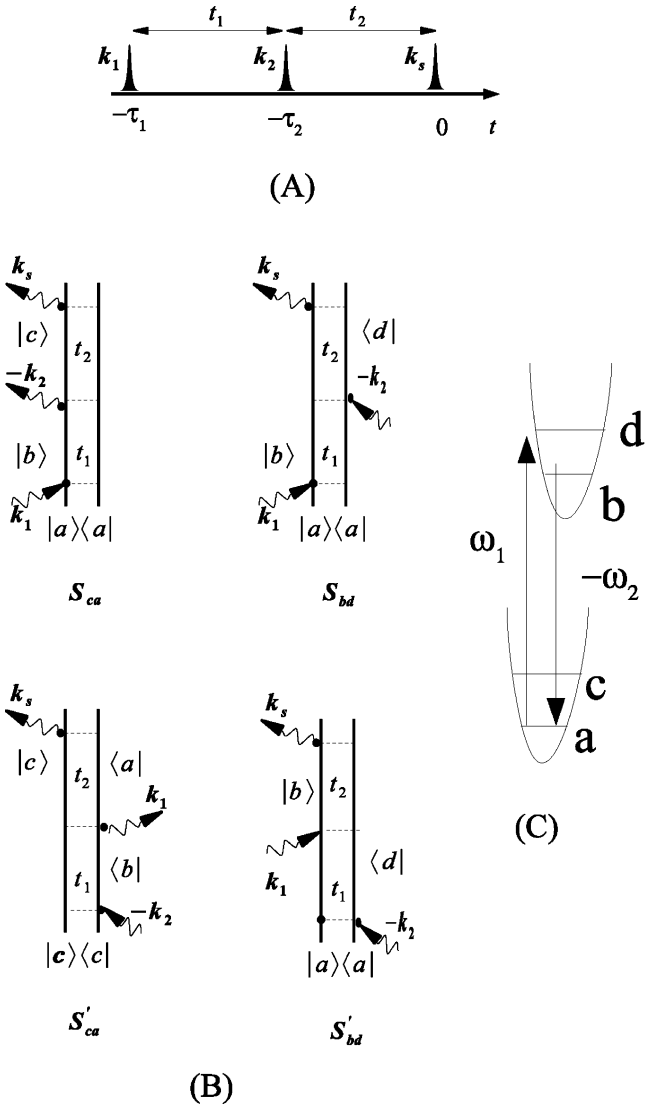

Figure 1. (A) Pulse sequence for a DFG experiment. (B) All Liouville space pathways contributing to the second-order response within the RWA. For well separated impulsive pulses where $\mathbf{k}_1$ comes first, $\mathbf{k}_{\mathrm{I}} = \mathbf{k}_1 - \mathbf{k}_2$ selects pathways S_{ca} and S_{bd}, whereas $\mathbf{k}_{\mathrm{II}} = -\mathbf{k}_1 + \mathbf{k}_2$ selects pathways S'_{ca} and S'_{bd}. For coincident pulses all four pathways contribute. (C) level scheme for the electronically resonant DFG experiment.

where t_1 is the time interval between the two interactions with the input fields and t_2 is the time interval between the second interaction and detection of the signal (Figure 1(A)). $S^{(2)}$ is given by[21]

$$S^{(2)}(t_2, t_1) = \left(\frac{i}{\hbar}\right)^2 \theta(t_2)\theta(t_1)\sum_{\alpha=1}^{2}[Q_\alpha(t_2, t_1) + Q_\alpha^*(t_2, t_1)] \quad (2)$$

with

$$Q_1 = \langle V(t_1 + t_2)V(t_1)V(0)\rangle \quad (3)$$

$$Q_2 = -\langle V(t_1)V(t_1 + t_2)V(0)\rangle \quad (4)$$

Here $V(t)$ is the dipole operator in the Heisenberg picture

$$V(t) = \exp\left(\frac{i}{\hbar}Ht\right)V\exp\left(-\frac{i}{\hbar}Ht\right) \quad (5)$$

where H is the molecular Hamiltonian.

We consider a multilevel system interacting with a bath, described by the Hamiltonian

$$H = \hbar\sum_\nu |\nu\rangle\left(\omega_\nu - i\frac{\gamma_\nu}{2} + q_\nu^{(c)}\right)\langle\nu| \quad (6)$$

Here $|\nu\rangle$ ($\nu = m, n, k...$) are the system eigenstates with eigenvalues $\hbar\omega_\nu$ and inverse lifetime γ_ν. The bath consists of harmonic modes and $q_\nu^{(c)}$ are collective Brownian oscillator bath coordinates.[21] The dipole operator is

$$\mathbf{V} = \sum_{\nu\nu'}|\nu'\rangle\mu_{\nu'\nu}\langle\nu| \quad (7)$$

where $\mu_{\nu'\nu}$ is the transition dipole between the states ν' and ν. The three-point correlation functions can be calculated exactly for this model using the second-order cumulant expansion following the procedure of[28]

$$Q_1(t_2, t_1) = \sum_{mnk}\mu_{km}\mu_{nk}\mu_{mn}W_m \exp(-i\omega_{nm}t_1 - \gamma_{nm}t_1)$$
$$\exp(-i\omega_{km}t_2 - \gamma_{km}t_2)\exp\Big(-\frac{1}{2}(g_{km}(t_1 + t_2) + g_{mn}(t_1 + t_2) -$$
$$g_{kn}(t_1 + t_2) - g_{mn}(t_2) + g_{mk}(t_2) + g_{kn}(t_2) - g_{km}(t_1) +$$
$$g_{kn}(t_1) + g_{nm}(t_1))\Big) \quad (8)$$

$$Q_2(t_2, t_1) = -\sum_{mnk}\mu_{km}\mu_{nk}\mu_{mn}W_m \exp(-i\omega_{nm}t_1 - \gamma_{nm}t_1)$$
$$\exp(-i\omega_{nk}t_2 - \gamma_{nk}t_2)\exp\Big(-\frac{1}{2}(g_{km}(t_1) + g_{mn}(t_1) - g_{kn}(t_1) -$$
$$g_{mn}^*(t_2) + g_{mk}^*(t_2) + g_{mn}^*(t_2) - g_{km}(t_1 + t_2) + g_{kn}(t_1 + t_2) +$$
$$g_{nm}(t_1 + t_2))\Big) \quad (9)$$

where W_m is the equilibrium population of level m, and $\gamma_{mn} = 1/2(\gamma_m + \gamma_n)$. The line shape function for the transition between levels m and n g_{mn} is given by

$$g_{mn}(t) = \int_0^t \mathrm{d}t' \int_0^{t'} \mathrm{d}t'' \, C_{mn}(t'') \quad (10)$$

where C_{mn} is the two time correlation function of the collective bath coordinate $q_{mn}^{(c)}(t) = q_m^{(c)}(t) - q_n^{(c)}(t)$

$$C_{mn}(t) = \frac{1}{\hbar}\langle q_{mn}^{(c)}(t)q_{mn}^{(c)}(0)\rangle \quad (11)$$

The spectral density of the collective coordinates $q_{mn}^{(c)}$ is defined as

$$C''_{mn}(\omega) = \frac{i}{2}\int_{-\infty}^{\infty}\mathrm{d}t\exp[i\omega t]\,\langle[q_{mn}^{(c)}(t), q_{mn}^{(c)}(0)]\rangle \quad (12)$$

Hereafter we use the overdamped Brownian oscillator model for the spectral density[21]

$$C''_{mn}(\omega) = 2\lambda_{mn}\frac{\omega\Lambda_{mn}}{\omega^2 + \Lambda_{mn}^2} \quad (13)$$

where λ_{mn} is the coupling strength of the mn transition with the bath and Λ_{mn} is the relaxation rate. In the high-temperature limit

($K_BT \gg \Lambda$) the two time correlation function for this model is given by[21]

$$C_{mn}(t) = \left[\frac{2K_BT\lambda_{mn}}{\hbar} - i\lambda_{mn}\Lambda_{mn}\right]\exp(-\Lambda_{mn}t) \quad (14)$$

where λ_{mn} represents the coupling strength of frequency fluctuations for the transition between levels m and n to the bath and Λ_{mn} is the relaxation rate of these fluctuations. Eq 10 then gives for the line shape function

$$g_{mn}(t) = \left(\frac{2\lambda_{mn}K_BT}{\hbar\Lambda_{mn}^2} - i\frac{\lambda_{mn}}{\Lambda_{mn}}\right)[\exp(-\Lambda_{mn}t) + \Lambda_{mn}t - 1] \quad (15)$$

The dimensionless parameter $\kappa_{mn} = \Lambda_{mn}/\Delta_{mn}$ [where $\Delta_{mn} = (2K_BT\lambda_{mn}/\hbar)^{1/2}$] represents the bath time scale. The total line width (fwhm) Γ_{mn} of the mn transition is given by the following Pade approximant in terms of the parameters Δ_{mn} and κ_{mn}:[21,29]

$$\frac{\Gamma_{mn}}{\Delta_{mn}} = \frac{2.355 + 1.76\kappa_{mn}}{1 + 0.85\kappa_{mn} + 0.88\kappa_{mn}^2} \quad (16)$$

In the $\kappa \gg 1$ (motional narrowing, fast bath) limit, $g_{mn}(t) = \hat{\Gamma}_{mn}t - i\lambda_{mn}t$ where $\hat{\Gamma}_{mn} \equiv \lambda_{mn}K_BT/\hbar\Lambda_{mn}$ is the homogeneous dephasing rate. In the opposite $\kappa \ll 1$ (inhomogeneous, slow bath) limit, we have $g_{mn}(t) = \Delta_{mn}^2t^2/2$ and Δ_{mn} is the line width.

III. Application to Electronically Resonant DFG

We now apply these results to a two electronic level model system: the ground (g) and the excited (e) levels, coupled to several vibrational modes (Figure 1C). This system can be represented by our multilevel Hamiltonian, where $|\nu\rangle$ now represents vibronic states. Hereafter, the indices $\nu = a, c$ will denote ground vibronic states and $\nu = b, d$ will denote excited vibronic states. We consider a resonant DFG experiment, whereby the two optical fields $\mathbf{k}_1$ and $\mathbf{k}_2$ are resonant with the electronic transition. The infrared signal generated at $\mathbf{k}_s = \mathbf{k}_1 - \mathbf{k}_2$ probes the dynamics of both ground and excited-state vibrational coherences induced in the system.

The applied electric field is

$$E(\boldsymbol{r}, t) = \epsilon_1(t + \tau_1)\exp(i\omega_1 t - i\mathbf{k}_1\cdot\boldsymbol{r}) + \epsilon_2(t + \tau_2)\exp(i\omega_2 t - i\mathbf{k}_2\cdot\boldsymbol{r}) + c.c. \quad (17)$$

Here $\mathbf{k}_j$, ω_j, and ϵ_j are the wavevector, frequency, and envelope of the pulse j. Pulses 1 and 2 peak at times $-\tau_1$ and $-\tau_2$, respectively, and the signal is detected around $t = 0$. We assume $\tau_1 > \tau_2$ (pulse 1 comes first) and define $t_1 = \tau_1 - \tau_2$ and $t_2 = \tau_2$ as the time intervals between the pulse centers (see Figure 1A). The pulses may overlap so that time ordering is not enforced. Substituting eq 17 in eq 1 gives

$$P(\mathbf{k}_1 - \mathbf{k}_2, t) = \int_0^\infty dt_2' \int_0^\infty dt_1' \exp(i(\omega_1 - \omega_2)t_2')S(t_2', t_1') [\exp(i\omega_1 t_1')\epsilon_1(t + \tau_1 - t_2' - t_1')\epsilon_2^*(t + \tau_2 - t_2') + \exp(-i\omega_2 t_1')\epsilon_2^*(t + \tau_2 - t_2' - t_1')\epsilon_1(t + \tau_1 - t_2')] \quad (18)$$

or

$$P(\mathbf{k}_1 - \mathbf{k}_2, t) = \int_{-\infty}^\infty d\omega_2 \int_{-\infty}^\infty d\omega_1 \chi^{(2)}(\omega_2 - \omega_1; -\omega_2, \omega_1) \epsilon_1(\omega_1)\epsilon_2^*(-\omega_2)\exp[-i(\omega_1 - \omega_2)t] \quad (19)$$

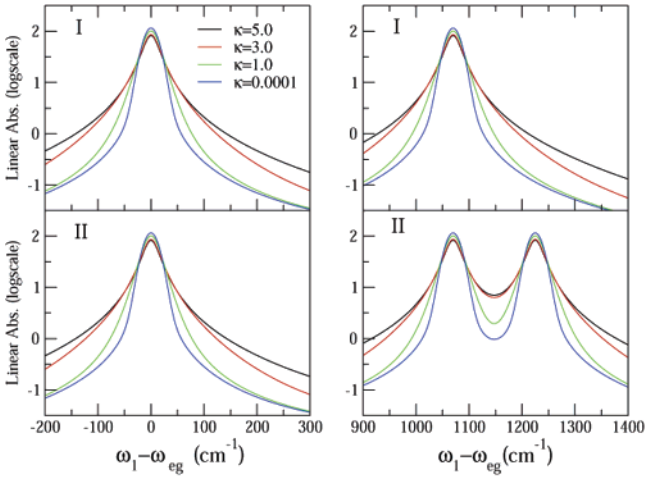

Figure 2. Linear absorption spectra for model I and model II as a function of the bath time scale parameter κ. Shown is the origin (left panel) and the $\omega_1 - \omega_{eg}$=1070 cm^{-1} resonance (right panel).

where

$$\chi^{(2)}(\omega_2 - \omega_1; -\omega_2, \omega_1) = \int_0^\infty dt_2' \int_0^\infty dt_1' S(t_2', t_1')\exp[i(\omega_1 - \omega_2)t_2'][\exp(i\omega_1 t_1') + \exp(-i\omega_2 t_1')]$$

$$\epsilon(\omega) = \int_{-\infty}^\infty d\tau\, \epsilon(\tau)\exp(i\omega\tau) \quad (20)$$

We next invoke the rotating wave approximation (RWA)[21] by neglecting off resonant terms with the field frequencies in eq 18. This gives

$$P(\mathbf{k}_1 - \mathbf{k}_2, t) = \left(\frac{i}{\hbar}\right)^2 \int_0^\infty dt_2' \int_0^\infty dt_1' \exp[i(\omega_1 - \omega_2)t_2'][(S_{ca}(t_2', t_1') + S_{bd}(t_2', t_1'))\exp[i\omega_1 t_1']\epsilon_1(t + \tau_1 - t_2' - t_1')\epsilon_2^*(t + \tau_2 - t_2') + (S'_{ca}(t_2', t_1') + S'_{bd}(t_2', t_1'))\exp[-i\omega_2 t_1'] \times \epsilon_2^*(t + \tau_2 - t_2' - t_1')\epsilon_1(t + \tau_1 - t_2')] \quad (21)$$

Double-sided Feynman diagrams for the four Liouville space pathways (S_{ca}, S_{bd}, S'_{ca}, and S'_{bd}) are given in Figure 1B, and the corresponding expressions are derived in Appendix A. DFG experiments can be performed with either ultrashort (broad-bandwidth) pulses or continuous wave (monochromatic) fields. These correspond to time-domain and frequency-domain experiments. The expressions simplify considerably for these limiting cases which are discussed in the following sections.

IV. Frequency-Domain (cw) Signals

In an ideal frequency-domain experiment, we assume monochromatic fields and eq 19 gives

$$P(\mathbf{k}_1 - \mathbf{k}_2, t) = \chi^{(2)}(\omega_2 - \omega_1; -\omega_2, \omega_1)\epsilon_1\epsilon_2^*\exp[-i(\omega_1 - \omega_2)t] \quad (22)$$

Using the RWA to pair up the various Liouville space contributions with the field permutations (as in eq 21), eq 20 gives

$$\chi^{(2)}(\omega_2 - \omega_1; -\omega_2, \omega_1) = \chi_{ca}^{(2)} + \chi_{bd}^{(2)} \quad (23)$$

where

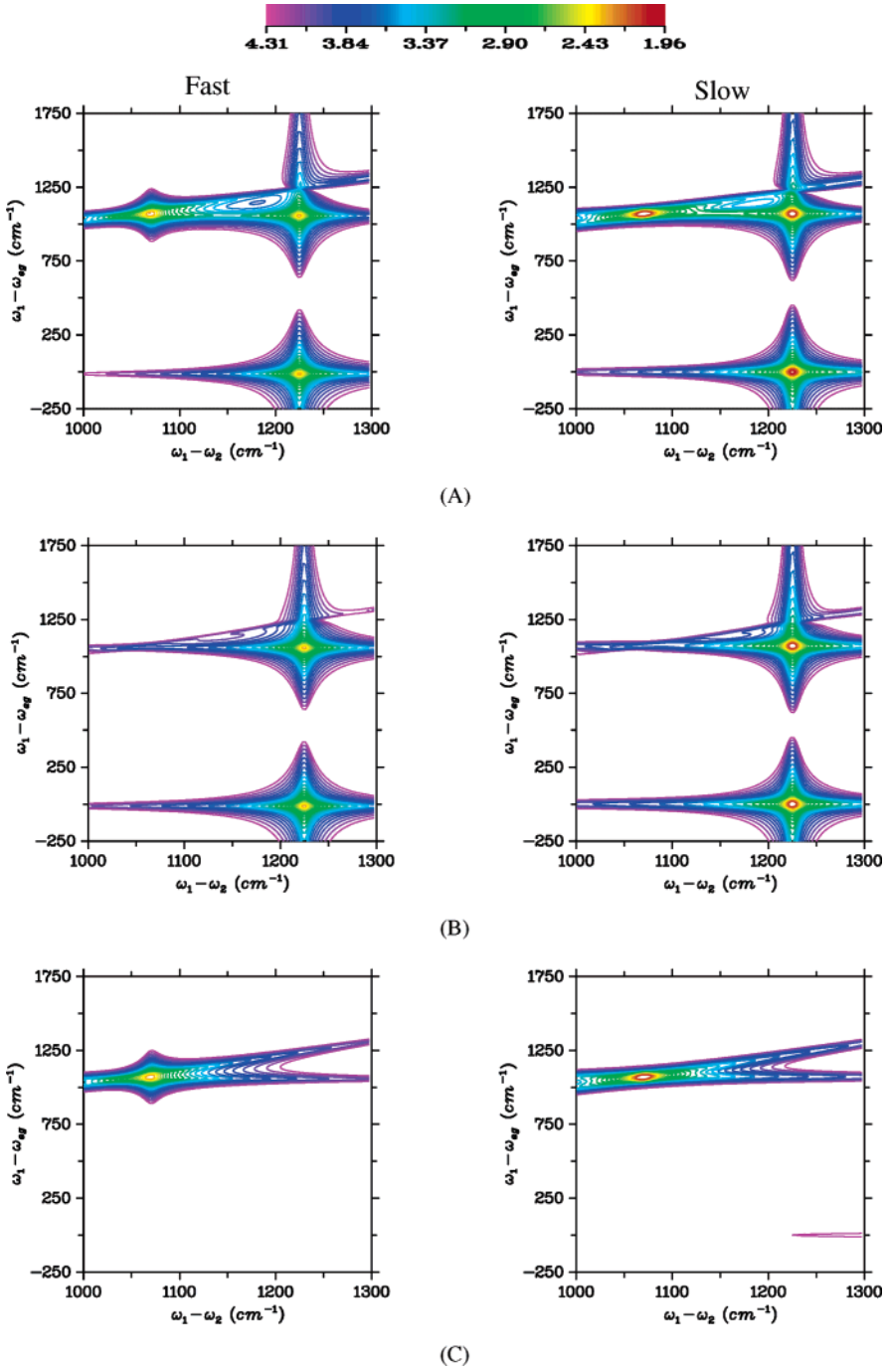

Figure 3. (A) Logscale 2D plots of frequency-domain homodyne signal ($\chi^{(2)}$, eq 23) showing resonances in the fast ($\kappa = 5$) and slow ($\kappa = 0.0001$) bath limits, (B) The ground-state contribution ($\chi^{(2)}_{ca}$ in eq 23). (C) The excited state contribution ($\chi^{(2)}_{bd}$ in eq 23).

$$\chi^{(2)}_{ca}(\omega_2 - \omega_1; -\omega_2, \omega_1) = \left(\frac{i}{\hbar}\right)^2 [S_{ca}(\omega_1 - \omega_2, \omega_1) + S'_{ca}(\omega_1 - \omega_2, -\omega_2)] \quad (24)$$

$$\chi^{(2)}_{bd}(\omega_2 - \omega_1; -\omega_2, \omega_1) = \left(\frac{i}{\hbar}\right)^2 [S_{bd}(\omega_1 - \omega_2, \omega_1) + S'_{bd}(\omega_1 - \omega_2, -\omega_2)] \quad (25)$$

with the double Fourier transform

$$S_m(\omega'_2, \omega'_1) = \int_0^\infty dt'_2 \int_0^\infty dt'_1 \exp[i\omega'_2 t'_2] \exp[i\omega'_1 t'_1] S_m(t'_2, t'_1) \quad (26)$$

S_{ca} and S'_{ca} (S_{bd} and S'_{bd}) given in Appendix A represent contributions to the response with ground state (excited state) resonances. In the fast bath limit ($\kappa \gg 1$), the line broadening function is given by: $g_{mn}(t) = \hat{\Gamma}_{mn} t - i\lambda_{mn} t$ and S_m are given by eq B1. We then get (see Appendix B)

$$\chi^{(2)}_{ca}(\omega_2 - \omega_1; -\omega_2, \omega_1) = \left(\frac{i}{\hbar}\right)^2 \sum_b \frac{1}{(\omega_1 - \omega_2) - \omega_{ca} + i(\gamma_{ca} + \hat{\Gamma}_{ca})} \left[\frac{W_a}{\omega_1 - \omega_{ba} + i(\gamma_{ba} + \hat{\Gamma}_{ba})} + \frac{W_c}{-\omega_2 - \omega_{cb} + i(\gamma_{cb} + \hat{\Gamma}_{cb})}\right] \quad (27)$$

$$\chi^{(2)}_{bd}(\omega_2-\omega_1;-\omega_2,\omega_1)=$$
$$-\left(\frac{i}{\hbar}\right)^2\sum_a\left[1+\frac{i(\gamma_a+\hat{\Gamma}_{ba}+\hat{\Gamma}_{ad}-\hat{\Gamma}_{bd})}{(\omega_1-\omega_2)-\omega_{bd}+i(\gamma_{bd}+\hat{\Gamma}_{bd})}\right]$$
$$\frac{W_a}{(\omega_1-\omega_{ba}-i(\gamma_{ba}+\hat{\Gamma}_{ba}))(-\omega_2-\omega_{ad}+i(\gamma_{ad}+\hat{\Gamma}_{ad}))} \quad (28)$$

This expression shows that, if the system is initially in the vibrational ground state ($\gamma_a = 0$), the excited state "*bd*" resonance will vanish in the absence of pure dephasing ($\hat{\Gamma}_{ba} + \hat{\Gamma}_{ad} - \hat{\Gamma}_{bd} = 0$). Pure dephasing is absent for our model in the slow bath limit $\kappa \ll 1$, which is also derived in Appendix B. For intermediate κ, the excited-state resonances will show a partial cancellation. The line shapes of excited-state resonances thus carry information about the bath time scales.

To demonstrate these effects, we have performed numerical simulations. We first consider an electronic two-level system with a single vibrational mode (model I). All electronic and vibrational transitions are allowed and their dipole strength is set to 1.0. The 0−0 "*g*" to "*e*" transition frequency is ω_{eg}. The vibrational mode frequency is 1225 cm^{-1} in "*g*" and 1070 cm^{-1} in "*e*". All states, excluding the ground vibrational state in "*g*" have the same inverse lifetime of $\gamma = 4$ cm^{-1}. The system is initially in the ground state ($a = 0$, $\gamma_a = 0$ cm^{-1}) in "*g*". The fwhm for all vibrational transitions (eq 16) is $\Gamma = 5$ cm^{-1} and for all electronic transitions is $\Gamma = 30$ cm^{-1}. The mode frequencies were chosen to match those observed in recent DFG experiments on myoglobin.[19] Other parameters such as the lifetime and dephasing rates represent typical literature values. All simulations were performed at room temperature (300 K) where W_a vanishes for $a \neq 0$. Figure 2 (top row) displays the linear absorption for this model showing two peaks corresponding to the vibrational levels in e showing the effect of the bath time scale on the line shape. As κ is decreased, the line shape changes from a Lorentzian to a Gaussian. Figure 3 displays 2D frequency-frequency contour plots of the absolute value cw signals (eq 23) with the difference frequency $\omega_1 - \omega_2$ along the *x* axis and the excitation frequency ω_1 along the *y* axis. The plots show an excited-state resonance at ($\omega_1 - \omega_{eg}$, $\omega_1 - \omega_2$) = (1070, 1070) cm^{-1} and two ground-state resonances at (1070, 1225) cm^{-1} and (1225, 1225) cm^{-1}. Eqs 27 and 28 show that in the fast bath limit ($\kappa = 5.0$) $\chi^{(2)}_{ca} \propto 1/(\omega_1 - \omega_2 - \omega_{ca})$ and $\chi^{(2)}_{bd} \propto \hat{\Gamma}/(\omega_1 - \omega_2 - \omega_{bd})$. In the slow bath limit, eq B3 shows that the excited-state contribution $\chi^{(2)}_{bd}$ does not contain a vibrational resonance. This implies that as the visible pulse frequency $\omega_1 - \omega_{eg}$ is detuned away from the electronic resonance the signal must vanish along $\omega_1 - \omega_2$=1070 cm^{-1} (Figure 3, parts A and C).The ground-state resonances do not show this cancellation (Figure 3, parts A and B). In Figures 4 and 5, we present sections of the contour plots to show the variation of DIR with κ. Figure 4 shows a slice of the 2D contour plot along $\omega_1 - \omega_2$ at $\omega_1 - \omega_{eg} = 1200$ cm^{-1} for different values of κ. Figure 5 depicts slices along ω_1 when $\omega_1 - \omega_2$ is tuned to the ground/excited-state resonances for different values of κ. These show the sensitivity of the excited-state resonance line shape to the bath time scale. Figure 4 shows that the excited-state resonance becomes weaker as κ is decreased. In Figure 5 the excited-state line shape shows a much sharper drop in the tails with decreasing κ as compared with the ground-state resonance.

We next consider model II with two vibrational modes (1070 and 1225 cm^{-1}) with identical frequencies in state "*g*" and "*e*".

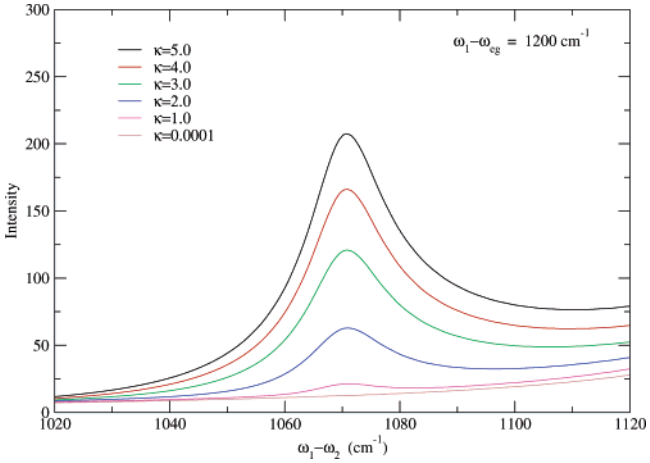

Figure 4. Slices of the 2D contour plots in Figure 3 at $\omega_1 - \omega_{eg} = 1200$ cm^{-1} taken at different values of κ.

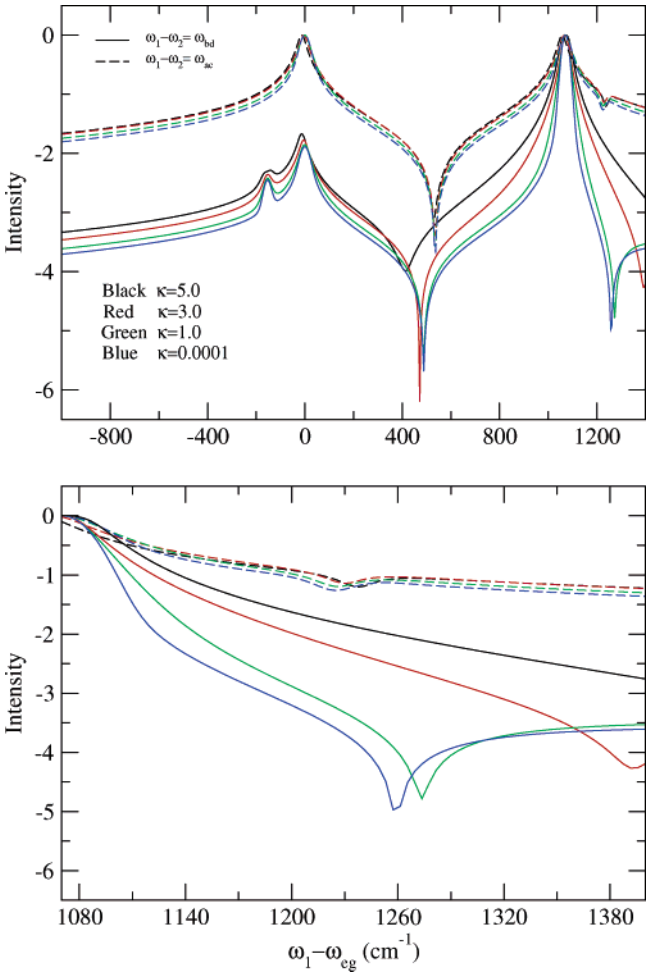

Figure 5. Logscale plots of the frequency-domain signal as a function of the excitation frequency ω_1 when $\omega_1 - \omega_2$ is tuned to ground (dotted lines) and excited (solid lines) state vibronic resonances. The lower panel shows the signal at the tail of the excited-state resonance at $\omega_1 - \omega_{eg} = 1070$ cm^{-1}.

It has the same pair of frequencies as model I, but the origin of the two frequencies is different (ground vs excited state coherences). All other parameters are the same. Figure 2 (bottom row) shows the linear absorption for this model. Figure 6 shows the (A) absolute value and (B) real parts of frequency−frequency contour plots for the cw signal in the fast bath limit. The negative ground state resonances can be easily distinguished

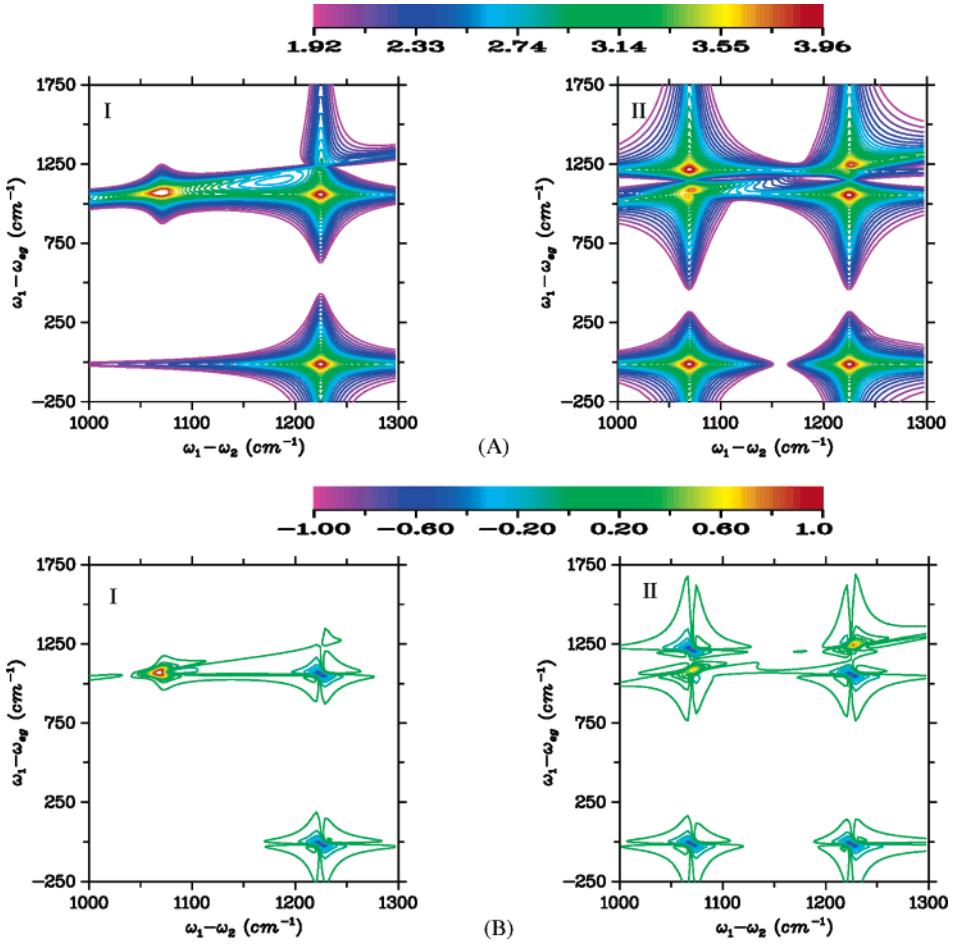

Figure 6. (A) Absolute value (logscale) and (B) real 2D plots for the CW signal (eq 23) in the fast bath limit as applied to the two model systems described in the section IV.

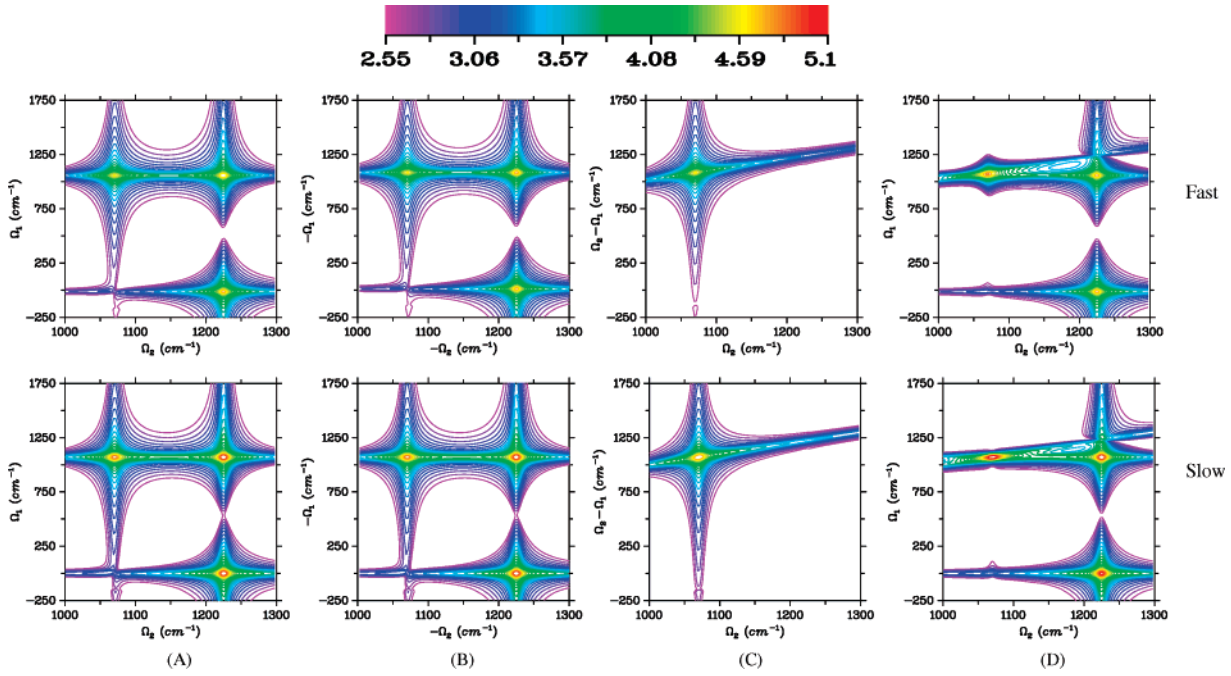

Figure 7. Absolute value (logscale) 2D plots of $P_{\mathrm{I}}(\Omega_2, \Omega_1)$ and $P_{\mathrm{II}}(\Omega_2', \Omega_1')$ (eq 32 with eqs 30 and 31) showing ground and excited-state resonances in the fast ($\kappa = 5$) and slow ($\kappa = 0.0001$) bath limits. The pulse frequencies are centered at $\omega_1 = \omega_{eg}$ and $\omega_1 - \omega_2 = 0$ cm^{-1}. Signals for two time-domain experiments and their superposition are displayed: (A) $\mathbf{k}_{\mathrm{I}} = \mathbf{k}_1 - \mathbf{k}_2$; (B) $\mathbf{k}_{\mathrm{II}} = \mathbf{k}_2 - \mathbf{k}_1$; (C) $P_{\mathrm{II}}(\Omega_2, \Omega_2 - \Omega_1)$; and (D) (A) + (C).

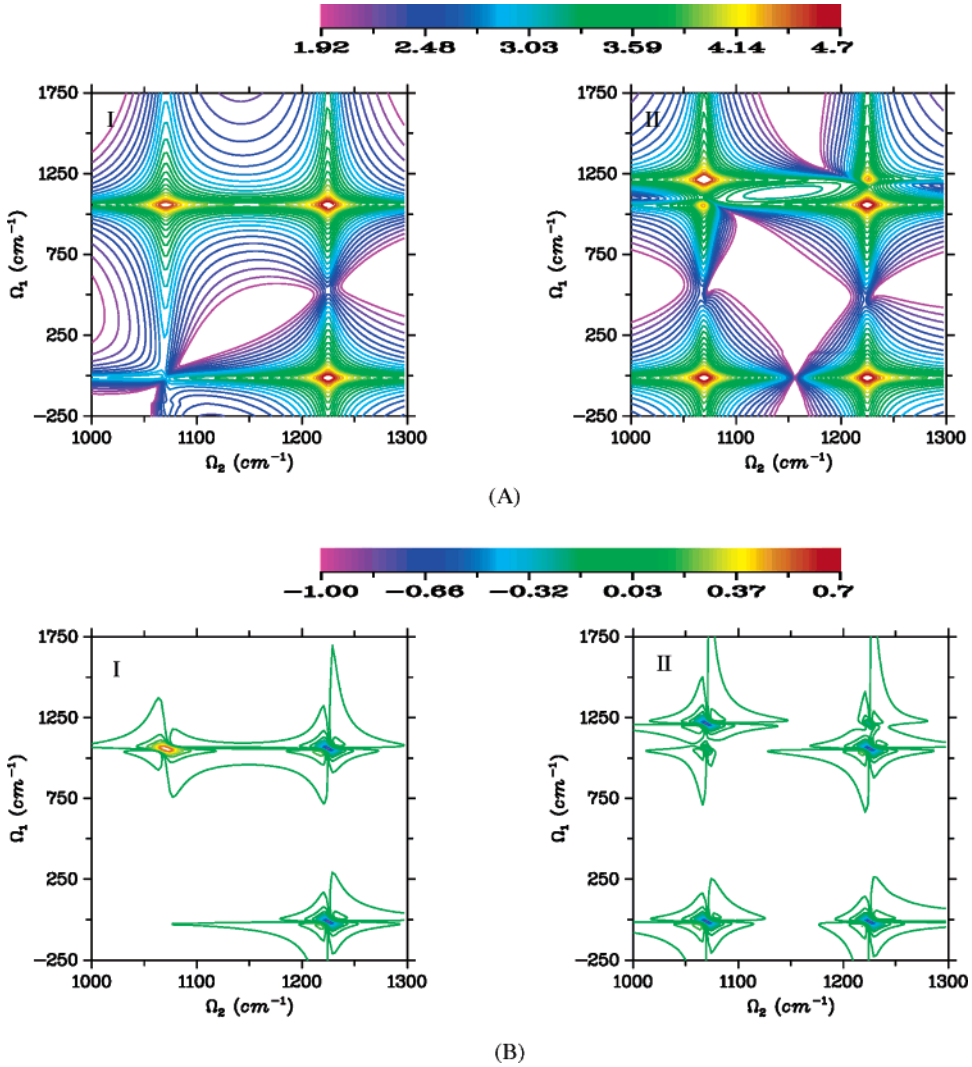

Figure 8. Same as Figure 6 but for impulsive input pulses (technique $\mathbf{k}_{\mathrm{I}}$ (eqs 32 and 30) with $\omega_1 = \omega_{eg}$ and $\omega_1 - \omega_2 = 0$ cm^{-1}).

from the positive excited-state resonances. The signals for the two models are different. For model I, the ground and the excited-state resonances have comparable magnitudes, but for model II, the excited-state resonances are weaker due to a partial cancellation with ground-state resonances. In the positive ($\omega_1 - \omega_2$, ω_1) quadrant, we expect a single peak along ω_1 axis for each excited resonance along $\omega_1 - \omega_2$ and two peaks for each ground state resonance. Model I clearly shows two different frequencies corresponding to the ground and excited states. For model II, we see that both resonances along $\omega_1 - \omega_2$ originate from ground and excited electronic states.

V. Time-Domain (Impulsive) Signals

In time-domain experiments, the time delay between the pulses can be controlled and scanned. We thus express the signals in terms of the delays t_1 and t_2. We have calculated the two possible signals $\mathbf{k}_I = \mathbf{k}_1 - \mathbf{k}_2$ and $\mathbf{k}_{II} = \mathbf{k}_2 - \mathbf{k}_1$

$$P_I(t_2, t_1) = \left(\frac{i}{\hbar}\right)^2 \int_0^\infty dt_2' \int_0^\infty dt_1' \exp(i(\omega_1 - \omega_2)t_2') [(S_{ca}(t_2', t_1') + S_{bd}(t_2', t_1')) \exp(i\omega_1 t_1')\epsilon_1(t_1 + t_2 - t_2' - t_1')\epsilon_2^*(t_2 - t_2') + (S'_{ca}(t_2', t_1') + S'_{bd}(t_2', t_1')) \exp(-i\omega_2 t_1')\epsilon_2^*(t_2 - t_2' - t_1') \times \epsilon_1(t_1 + t_2 - t_2')] \quad (29)$$

and $P_{II}(t_2, t_1) = P_I^*(t_2, t_1)$ In an ideal, impulsive (time-domain) experiment the field envelopes in eqs 21 and 29 are represented by delta functions $\epsilon_1(t) = \epsilon_2(t) = \delta(t)$. For well-separated pulses, a specific time ordering is imposed leading to either technique $\mathbf{k}_{\mathrm{I}}$, selecting pathways S_{ca} and S_{bd} or technique $\mathbf{k}_{\mathrm{II}}$ selecting pathways S'_{ca} and S'_{bd}. Using eq 29 and its complex conjugate, we have

$$P_{\mathrm{I}}(t_2, t_1) = \left(\frac{i}{\hbar}\right)^2 \exp(i(\omega_1 - \omega_2)t_2) \exp(i\omega_1 t_1) [S_{ca}(t_2, t_1) + S_{bd}(t_2, t_1)] \quad (30)$$

and

$$P_{\mathrm{II}}(t_2, t_1) = \left(\frac{i}{\hbar}\right)^2 \exp(-i(\omega_1 - \omega_2)t_2) \exp(-i\omega_1 t_1) [S'_{ca}(t_2, t_1) + S'_{bd}(t_2, t_1)] = P_I^*(t_2, t_1) \quad (31)$$

In this case, only one ground-state pathway and one excited-state pathway contribute. Eq 28 shows that DIR results from the sum of two excited-state pathways. Thus, each individual time-domain experiment will not show DIR. However, the frequency-domain interference can be recovered by adding signals from impulsive, time-domain techniques: $\mathbf{k}_{\mathrm{I}}$ and

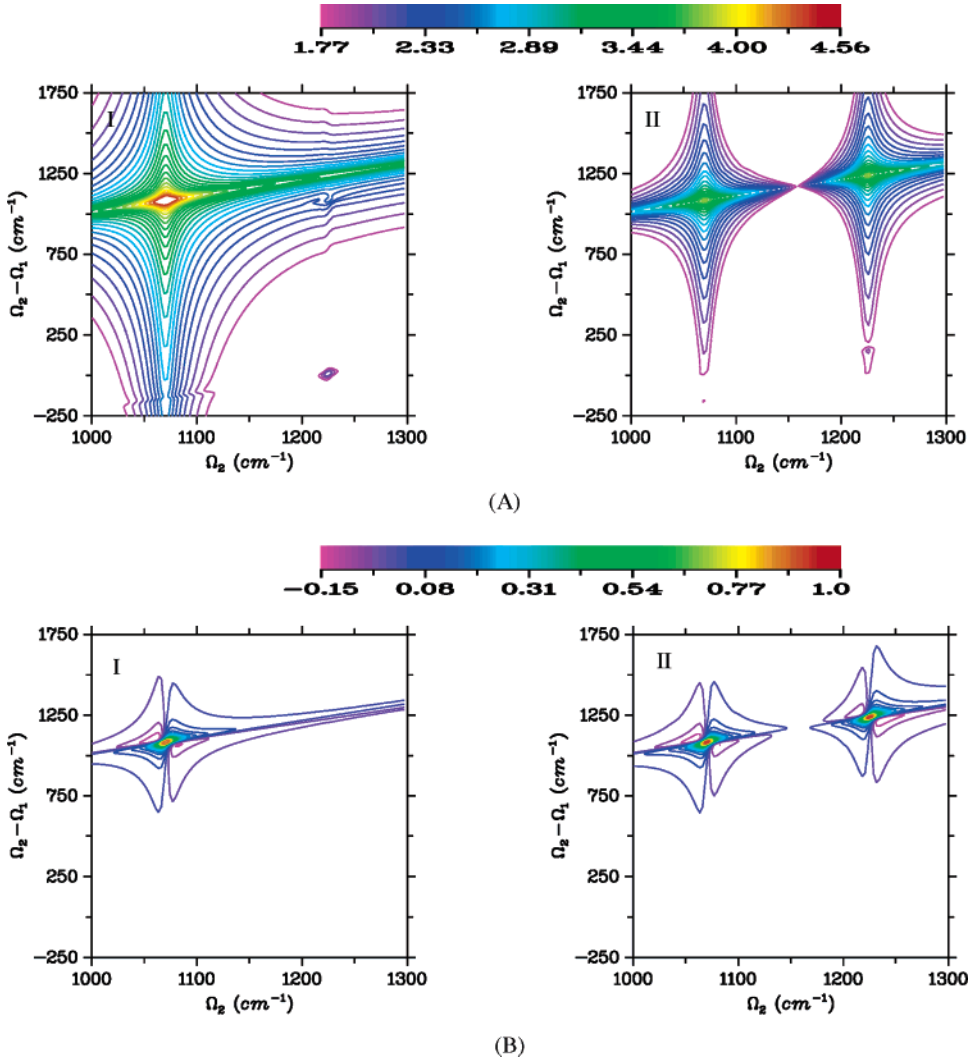

Figure 9. Same as Figure 6 but for the impulsive technique $\mathbf{k}_{II}$ (eqs 32 and 31).

$\mathbf{k}_{II}$ with well separated pulses (see Appendix C) which select mutually exclusive pathways.

We shall display these signals in the frequency-domain by taking a Fourier transform with respect to the time intervals

$$P_I(\Omega_2, \Omega_1) = \int_0^\infty dt_2 \exp(i\Omega_2 t_2) \int_0^\infty dt_1 \exp(i\Omega_1 t_1) P_I(t_2, t_1) \quad (32)$$

and similarly for P_{II}. Figure 7, parts A and B, shows the absolute value (logscale) 2D contour plots (eq 32 together with 30 and 31) in the fast and slow bath limits. Since the signals $P_I(t_2, t_1)$ and $P_{II}(t_2, t_1)$ are complex conjugates, the $\mathbf{k}_I$ signal in the positive (Ω_2, Ω_1) quadrant is the same as the $\mathbf{k}_{II}$ signal in the negative (Ω_2', Ω_1') quadrant. The individual signals show no interference. Figure 7C shows the $P_{II}(\Omega_2' = \Omega_2, \Omega_1' = \Omega_2 - \Omega_1)$ which when added with the $\mathbf{k}_I$ signal reproduces the frequency-domain interference as shown in Figure 7D. In Figure 7A, the ground-state resonances are stronger than the excited-state resonances. Eqs A1 and A2 show that the line width of the "*ac*" resonance is smaller than the "*bd*" resonance due to the finite lifetime of the vibrational ground state in "*e*". The reverse is true in Figure 7C where the excited-state resonances are stronger (the ground-state resonances cannot be seen on this scale). Eqs A3 and A4 show that the ground-state pathways are weighted by the populations W_c (for positive values of Ω_2, c cannot be the ground vibrational state) which are weak at room temperature for $c \neq 0$.

Interference effects between ground and excited-state pathways as seen in the cw experiments for model II can be further analyzed by examining the impulsive signal. Figure 8 shows the real and the absolute value (logscale) plots for the impulsive technique $\mathbf{k}_I$. Note that the real part of the signal for model II shows only negative peaks. As discussed earlier for model I, the ground-state resonances are narrower than the excited-state resonances and the partial cancellation of ground and excited-state resonances in model II leads to negative peaks. Figure 9 shows similar plots for the $\mathbf{k}_{II}$. Here the effect is the opposite: For model II, interference between ground and excited state pathways will necessarily lead to positive peaks. We further note that the disparity between ground and excited-state pathway contributions for $\mathbf{k}_{II}$ is greater than that for $\mathbf{k}_I$, which implies that the interference between the ground and excited-state cw resonances will also lead to positive peaks, as observed earlier.

VI. Temporally Overlapping Pulses

For finite pulses, both field permutations in eq 21 contribute (with unequal weights), and it should be possible to excite transitions within a certain bandwidth. The signal depends on

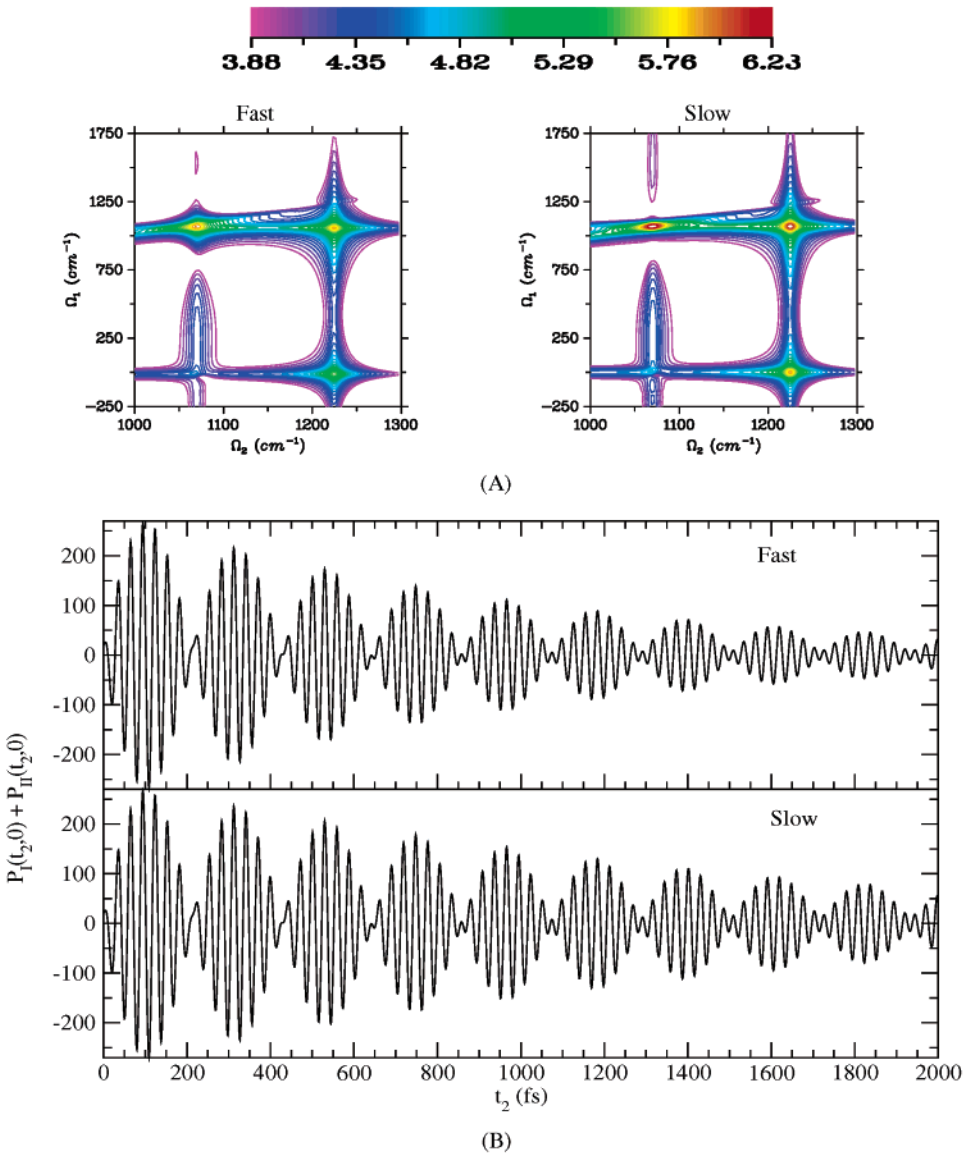

Figure 10. Absolute value (logscale) 2D plots for Gaussian input pulses with a finite pulse width, $\sigma = 10$ fs (eq 29 and its complex conjugate) in the fast ($\kappa = 5$) and slow ($\kappa = 10^{-4}$) bath limits. The input pulses are centered at $\omega_1 = \omega_{eg}$ and $\omega_1 - \omega_2 = 0$ cm^{-1}. (A) 2D frequency-frequency contour plots of the superposition $\mathbf{k}_I + \mathbf{k}_{II}$ for well separated pulses. (B) Time-domain signal for a single input pulse ($t_1 = 0$).

the time delay and carrier frequency of both pulses. As the pulse bandwidth increases from the impulsive limit to approach the cw limit, the signal becomes increasingly independent of the delay between the pulses and increasingly dependent on the field frequencies. Figure 10 shows the signal for finite width Gaussian pulses in the fast and slow bath limit for model I. The two input pulses were assumed to have the same temporal width (σ), and we have computed both $\mathbf{k}_{\mathrm{I}}$ and $\mathbf{k}_{\mathrm{II}}$ signals (eq 29 and its complex conjugate). For $\sigma = 10$ fs, $\mathbf{k}_{\mathrm{I}}$ and $\mathbf{k}_{\mathrm{II}}$ select mutually exclusive pathways. We show the superposition of these two signals in Figure 10A. In the DFG experiments on myoglobin,[19] the two interactions take place with a single input pulse. This situation is shown in Figure 10B for $\sigma = 10$ fs as applied to model I. As seen from eq 21, if the pulses are coincident ($t_1 = 0$), all four pathways will be selected. If the two pulses are coincident and impulsive, then both sets of pathways would contain no electronic coherence (since the system would not have time to evolve between the two interactions). The two excited-state contributions should be equivalent (in Figure 1B S_{bd} and S'_{bd} differ only by the electronic coherence in the first time interval). The time-resolved signals in Figure 10B show beats at the frequency difference between ground and excited-state mode frequencies. Multidimensional plots of experiments carried out with well separated pulses (Figure 10A) give additional information about the bath time scale.

In conclusion, we have computed the DFG signal for a model level scheme of a two electronic level system with several vibrational modes coupled to a harmonic bath represented by the overdamped Brownian oscillator model. Our calculations show that the bath time scales have clear signatures in DFG experiments when the pulses overlap, due to the cancellation of excited-state vibrational resonances by interference of Liouville space pathways. Time-domain (impulsive) techniques do not show this interference as these experiments impose a specific pulse ordering. The interference is recovered by combining two impulsive experiments $\mathbf{k}_{\mathrm{I}}$ and $\mathbf{k}_{\mathrm{II}}$ with well separated pulses. Experiments with coincident pulses should also show DIR interference effects provided the pulse width is of the order of the electronic dephasing time scale of the system. Comparison of time- and frequency-domain DFG signals for

two different model systems highlights the sensitivity of the DFG signal to the ground and excited-state coherences.

Acknowledgment. This article is based upon work supported by the National Institutes of Health under Grant Number CHE-0132571, the National Science Foundation (GM59230-01A3), and the Air Force Office of Scientific Research (FA9550-04-1-0332). This support is gratefully acknowledged. We also thank Prof. J. -L. Martin, Dr. M.-L. Groot, and Dr. J. -C. Lambry for useful discussions regarding their myoglobin experiments.

Appendix A: Second-Order Response Function

Using eqs 8 and 9 and Figure 1B, we can separate the terms with ground and excited-state resonances

$$S_{ca}(t_2, t_1) = \sum_{abc} W_a \mu_{ca}\mu_{bc}\mu_{ab} \exp(-i\omega_{ba}t_1 - \gamma_{ba}t_1) \exp(-i\omega_{ca}t_2 - \gamma_{ca}t_2) \exp\left(-\frac{1}{2}(g_{ca}(t_1+t_2) + g_{ab}(t_1+t_2) - g_{cb}(t_1+t_2) - g_{ab}(t_2) + g_{ac}(t_2) + g_{cb}(t_2) - g_{ca}(t_1) + g_{cb}(t_1) + g_{ba}(t_1))\right) \quad \text{(A1)}$$

$$S_{bd}(t_2, t_1) = -\sum_{abd} W_a \mu_{da}\mu_{bd}\mu_{ad} \exp(-i\omega_{ba}t_1 - \gamma_{ba}t_1) \exp(-i\omega_{bd}t_2 - \gamma_{bd}t_2) \exp\left(-\frac{1}{2}(g_{da}(t_1) + g_{ab}(t_1) - g_{db}(t_1) - g^*_{ab}(t_2) + g^*_{ad}(t_2) + g^*_{db}(t_2) - g_{da}(t_1+t_2) + g_{db}(t_1+t_2) + g_{ba}(t_1+t_2))\right) \quad \text{(A2)}$$

$$S'_{ca}(t_2, t_1) = \sum_{abc} W_c \mu_{ca}\mu_{bc}\mu_{ab} \exp(-i\omega_{cb}t_1 - \gamma_{cb}t_1) \exp(-i\omega_{ca}t_2 - \gamma_{ca}t_2) \exp\left(-\frac{1}{2}(g_{ca}(t_1+t_2) + g_{bc}(t_1+t_2) - g_{ba}(t_1+t_2) - g_{bc}(t_2) + g_{ac}(t_2) + g_{ba}(t_2) - g_{ca}(t_1) + g_{ba}(t_1) + g_{cb}(t_1))\right) \quad \text{(A3)}$$

$$S'_{bd}(t_2, t_1) = -\sum_{abd} W_a \mu_{da}\mu_{bd}\mu_{ad} \exp(-i\omega_{ad}t_1 - \gamma_{ad}t_1) \exp(-i\omega_{bd}t_2 - \gamma_{bd}t_2) \exp\left(-\frac{1}{2}(g_{ab}(t_1) + g_{da}(t_1) - g_{db}(t_1) - g^*_{da}(t_2) + g^*_{ba}(t_2) + g^*_{db}(t_2) - g_{ab}(t_1+t_2) + g_{db}(t_1+t_2) + g_{ad}(t_1+t_2))\right) \quad \text{(A4)}$$

Appendix B: Frequency-Domain (cw) Signal

Below we derive closed expressions for the frequency-domain signal in the fast and the slow bath limits of the overdamped Brownian oscillator model

1. Fast Bath. For $\kappa \gg 1$, the line broadening function is given by $g(t) = \hat{\Gamma}t + i\lambda t$. Substituting this in eqs A1−A4, we get (assuming the temperature is high enough to neglect the stokes shift)

$$S_{ca}(t_2, t_1) = \sum_{abc} W_a \mu_{ca}\mu_{bc}\mu_{ab} \exp(-i\omega_{ba}t_1 - \gamma_{ba}t_1 - \hat{\Gamma}_{ba}t_1) \exp(-i\omega_{ca}t_2 - \gamma_{ca}t_2 - \hat{\Gamma}_{ca}t_2)$$

$$S_{bd}(t_2, t_1) = -\sum_{abd} W_a \mu_{da}\mu_{bd}\mu_{ad} \exp(-i\omega_{ba}t_1 - \gamma_{ba}t_1 - \hat{\Gamma}_{ba}t_1) \exp(-i\omega_{bd}t_2 - \gamma_{bd}t_2 - \hat{\Gamma}_{bd}t_2)$$

$$S'_{ca}(t_2, t_1) = \sum_{abc} W_c \mu_{ca}\mu_{bc}\mu_{ab} \exp(-i\omega_{cb}t_1 - \gamma_{cb}t_1 - \hat{\Gamma}_{cb}t_1) \exp(-i\omega_{ca}t_2 - \gamma_{ca}t_2 - \hat{\Gamma}_{ca}t_2)$$

$$S'_{bd}(t_2, t_1) = -\sum_{abd} W_a \mu_{da}\mu_{bd}\mu_{ad} \exp(-i\omega_{ad}t_1 - \gamma_{ad}t_1 - \hat{\Gamma}_{ad}t_1) \exp(-i\omega_{bd}t_2 - \gamma_{bd}t_2 - \hat{\Gamma}_{bd}t_2) \quad \text{(B1)}$$

Substituting this into eqs 24 and 25 we get

$$\chi^{(2)}_{ca}(\omega_2 - \omega_1; -\omega_2, \omega_1) = \left(\frac{i}{\hbar}\right)^2 \sum_b \frac{1}{(\omega_1 - \omega_2) - \omega_{ca} + i(\gamma_{ca} + \hat{\Gamma}_{ca})} \left[\frac{W_a}{\omega_1 - \omega_{ba} + i(\gamma_{ba} + \hat{\Gamma}_{ba})} + \frac{W_c}{-\omega_2 - \omega_{cb} + i(\gamma_{cb} + \hat{\Gamma}_{cb})}\right] \quad \text{(B2)}$$

and

$$\chi^{(2)}_{bd}(\omega_2 - \omega_1; -\omega_2, \omega_1) = -\left(\frac{i}{\hbar}\right)^2 \sum_a \frac{W_a}{(\omega_1 - \omega_2) - \omega_{bd} + i(\gamma_{bd} + \hat{\Gamma}_{bd})} \left[\frac{1}{\omega_1 - \omega_{ba} + i(\gamma_{ba} + \hat{\Gamma}_{ba})} + \frac{1}{-\omega_2 - \omega_{ad} + i(\gamma_{ad} + \hat{\Gamma}_{ad})}\right] \quad \text{(B3)}$$

Assuming that "a" is the ground state ($\gamma_a = 0$), eq B3 can be rearranged[21] to give eq 28 which shows that the excited state "bd" resonance vanishes in the absence of pure dephasing. The ground-state term does not show such cancellation.

2. Slow Bath. For $\kappa \ll 1$, the line broadening function has the form: $g(t) = \Delta^2 t^2/2$ Substituting this into eqs A1−A4 gives

$$S_{ca}(t_2, t_1) = \sum_{abc} W_a \mu_{ca}\mu_{bc}\mu_{ab} \exp(-i\omega_{ba}t_1 - \gamma_{ba}t_1) \exp(-i\omega_{ca}t_2 - \gamma_{ca}t_2) f_1(t_2, t_1)$$

$$S_{bd}(t_2, t_1) = -\sum_{abd} W_a \mu_{da}\mu_{bd}\mu_{ad} \exp(-i\omega_{ba}t_1 - \gamma_{ba}t_1) \exp(-i\omega_{bd}t_2 - \gamma_{bd}t_2) f_2(t_2, t_1)$$

$$S'_{ca}(t_2, t_1) = \sum_{abc} W_c \mu_{ca}\mu_{bc}\mu_{ab} \exp(-i\omega_{cb}t_1 - \gamma_{cb}t_1) \exp(-i\omega_{ca}t_2 - \gamma_{ca}t_2) f_3(t_2, t_1)$$

$$S'_{bd}(t_2, t_1) = -\sum_{abd} W_a \mu_{da}\mu_{bd}\mu_{ad} \exp(-i\omega_{ad}t_1 - \gamma_{ad}t_1) \exp(-i\omega_{bd}t_2 - \gamma_{bd}t_2) f_4(t_2, t_1) \quad \text{(B4)}$$

where

$$f_1(t_2, t_1) = \exp\Big[-\frac{1}{2}(\Delta^2{}_{ba}t_1{}^2 + \Delta^2{}_{ca}t_2{}^2 + (\Delta_{ba}{}^2 + \Delta_{ca}{}^2 - \Delta_{cb}{}^2)t_1t_2)\Big]$$

$$f_2(t_2, t_1) = \exp\Big[-\frac{1}{2}(\Delta^2{}_{ba}t_1{}^2 + \Delta^2{}_{bd}t_2{}^2 + (\Delta_{ba}{}^2 + \Delta_{bd}{}^2 - \Delta_{ad}{}^2)t_1t_2)\Big]$$

$$f_3(t_2, t_1) = \exp\Big[-\frac{1}{2}(\Delta^2{}_{cb}t_1{}^2 + \Delta^2{}_{ca}t_2{}^2 + (\Delta_{cb}{}^2 + \Delta_{ca}{}^2 - \Delta_{ba}{}^2)t_1t_2)\Big]$$

$$f_4(t_2, t_1) = \exp\Big[-\frac{1}{2}(\Delta^2{}_{ad}t_1{}^2 + \Delta^2{}_{bd}t_2{}^2 + (\Delta_{ad}{}^2 + \Delta_{bd}{}^2 - \Delta_{ba}{}^2)t_1t_2)\Big] \quad \text{(B5)}$$

in this limit the expressions reduce to the isolated molecule (no pure dephasing) averaged over a Gaussian bivariate distribution of frequencies. Substituting this in eqs 24 and 25, we can express the ground and excited-state signals as a convolution of the single molecule transform and a bivariate distribution

$$\chi^{(2)}_{ca}(\omega_2 - \omega_1; -\omega_2, \omega_1) = \left(\frac{i}{\hbar}\right)^2 \sum_b \int_{-\infty}^{\infty} d\omega' \int_{-\infty}^{\infty} d\omega'' \,[(I_{ca}(\omega_1 - \omega_2 - \omega') \times I_{ba}(\omega_1 - \omega''))W_a G_1(\omega', \omega'') + (I_{ca}(\omega_1 - \omega_2 - \omega') \times I_{cb}(-\omega_2 - \omega''))W_c G_3(\omega', \omega'')] \quad \text{(B6)}$$

and

$$\chi^{(2)}_{bd}(\omega_2 - \omega_1; -\omega_2, \omega_1) = -\left(\frac{i}{\hbar}\right)^2 \sum_a \int_{-\infty}^{\infty} d\omega' \int_{-\infty}^{\infty} d\omega'' \, W_a[(I_{bd}(\omega_1 - \omega_2 - \omega') \times I_{ba}(\omega_1 - \omega''))G_2(\omega', \omega'') + (I_{bd}(\omega_1 - \omega_2 - \omega') \times I_{ad}(-\omega_2 - \omega''))G_4(\omega', \omega'')] \quad \text{(B7)}$$

where

$$I_{\nu\nu'}(\omega) = \frac{1}{\omega - \omega_{\nu\nu'} + i\gamma_{\nu\nu'}} \quad \text{(B8)}$$

and the G's are double Fourier transforms of the Gaussian bivariate distributions (eq B5)

$$G_i(\omega_m, \omega_n) = \int_{-\infty}^{\infty}\int_{-\infty}^{\infty} f_i(t_2, t_1) \exp(i\omega_m t_2) \exp(i\omega_n t_1) \, dt_2 \, dt_1 \quad \text{(B9)}$$

substituting eqs B5 in eq B9 we get

$$G_1(\omega', \omega'') = G_3(\omega', \omega'') = \left(\frac{4\pi^2}{\delta_g{}^2}\right) \exp\left[-\frac{1}{2\delta_g{}^2}(\Delta_{ba}{}^2(\omega')^2 + \Delta_{ca}{}^2(\omega'')^2 - (\Delta_{ba}{}^2 + \Delta_{ca}{}^2 - \Delta_{cb}{}^2)\omega'\omega'')\right] \quad \text{(B10)}$$

and

$$G_2(\omega', \omega'') = G_4(\omega', \omega'') = \left(\frac{4\pi^2}{\delta_e{}^2}\right) \exp\left[-\frac{1}{2\delta_e{}^2}(\Delta_{ba}{}^2(\omega')^2 + \Delta_{bd}{}^2(\omega'')^2 - (\Delta_{ba}{}^2 + \Delta_{bd}{}^2 - \Delta_{ad}{}^2)\omega'\omega'')\right] \quad \text{(B11)}$$

with

$$\delta_g{}^2 = 4\Delta_{ca}{}^2\Delta_{ba}{}^2 - (\Delta_{ca}{}^2 + \Delta_{ba}{}^2 - \Delta_{cb}{}^2)^2$$
$$\delta_e{}^2 = 4\Delta_{bd}{}^2\Delta_{ba}{}^2 - (\Delta_{bd}{}^2 + \Delta_{ba}{}^2 - \Delta_{ad}{}^2)^2 \quad \text{(B12)}$$

Using the above and $\omega_{ad} = \omega_{bd} - \omega_{ba}$, we obtain for the excited-state signal

$$\chi_{bd}{}^{(2)}(\omega_2 - \omega_1; -\omega_2, \omega_1) = -\sum_a \int_{-\infty}^{\infty} d\omega' \int_{-\infty}^{\infty} d\omega'' \, W_a I_{bd}(\omega_1 - \omega_2 - \omega') \left[\frac{1}{\omega_1 - \omega'' - \omega_{ba} + i\gamma_{ba}} + \frac{1}{(\omega_1 - \omega_2 - \omega' - \omega_{bd}) - (\omega_1 - \omega'' - \omega_{ba}) + i\gamma_{ad}}\right] G_2(\omega', \omega'') \quad \text{(B13)}$$

The expression in the square brackets is the same as eq 28 with no pure dephasing. This implies that there is no "*bd*" resonance in the slow bath limit.

Appendix C: Time-Domain (Impulsive) Signal

In this section, we show expressions for the time-domain signals $\mathbf{k}_{\mathrm{I}}$ and $\mathbf{k}_{\mathrm{II}}$ in the limiting cases of fast and slow baths. As with the frequency-domain expressions, we separate the ground and excited-state contributions

$$P_{\mathrm{I}}(t_2, t_1) = P_{ca}(\mathbf{k}_1 - \mathbf{k}_2, t_2, t_1) + P_{bd}(\mathbf{k}_1 - \mathbf{k}_2, t_2, t_1) \quad \text{(C1)}$$

$$P_{\mathrm{II}}(t_2, t_1) = P_{ca}(\mathbf{k}_2 - \mathbf{k}_1, t_2, t_1) + P_{bd}(\mathbf{k}_2 - \mathbf{k}_1, t_2, t_1) \quad \text{(C2)}$$

1. Fast Bath ($\kappa \gg 1$). *Case 1.* When the input pulses are time coincident, eq 29 along with eqs A1−A4 leads to

$$P_{ca}(\mathbf{k}_1 - \mathbf{k}_2, t_2, 0) = \exp(i(\omega_1 - \omega_2)t_2)2Re\left[\left(\frac{i}{\hbar}\right)^2 \sum_{abc} \mu_{ca}\mu_{bc}\mu_{ab}W_a \exp(-i\omega_{ca}t_2 - \gamma_{ca}t_2 - \hat{\Gamma}_{ca}t_2)\right] \quad \text{(C3)}$$

$$P_{bd}(\mathbf{k}_1 - \mathbf{k}_2, t_2, 0) = -\exp(i(\omega_1 - \omega_2)t_2)2Re\left[\left(\frac{i}{\hbar}\right)^2 \sum_{abd} \mu_{ad}\mu_{bd}\mu_{ba}W_{\mathrm{a}} \exp(-i\omega_{bd}t_2 - \gamma_{bd}t_2 - \hat{\Gamma}_{bd}t_2)\right] \quad \text{(C4)}$$

$$P_{\mathrm{II}}(t_2, 0) = P_{\mathrm{I}}^*(t_2, 0) \quad \text{(C5)}$$

Case 2. For the case where the input pulses are well separated in time, the Fourier transformed ground and excited-state time-domain signals are given by eq 32 along with eqs 30, 31, and

A1−A4. In the fast bath limit, these lead to

$$P_{ca}(\mathbf{k}_1-\mathbf{k}_2,\Omega_2,\Omega_1)=\left(\frac{i}{\hbar}\right)^2\sum_{abc}\frac{W_a}{\Omega_2-(\omega_{ca}-\omega_1+\omega_2)+i(\gamma_{ca}+\hat{\Gamma}_{ca})}\frac{1}{\Omega_1-(\omega_{ba}-\omega_1)+i(\gamma_{ba}+\hat{\Gamma}_{ba})}$$

$$P_{ca}(\mathbf{k}_2-\mathbf{k}_1,\Omega_2,\Omega_1)=\left(\frac{i}{\hbar}\right)^2\sum_{abc}\frac{W_c}{\Omega_2-(\omega_{ca}-\omega_1+\omega_2)+i(\gamma_{ca}+\hat{\Gamma}_{ca})}\frac{1}{\Omega_1-(\omega_{cb}-\omega_1)+i(\gamma_{cb}+\hat{\Gamma}_{cb})}$$

$$P_{bd}(\mathbf{k}_1-\mathbf{k}_2,\Omega_2,\Omega_1)=-\left(\frac{i}{\hbar}\right)^2\sum_{abd}\frac{W_a}{\Omega_2-(\omega_{bd}-\omega_1+\omega_2)+i(\gamma_{bd}+\hat{\Gamma}_{bd})}\frac{1}{\Omega_1-(\omega_{ba}-\omega_1)+i(\gamma_{ba}+\hat{\Gamma}_{ba})} \quad \text{(C6)}$$

$$P_{bd}(\mathbf{k}_2-\mathbf{k}_1,\Omega_2,\Omega_1)=-\left(\frac{i}{\hbar}\right)^2\sum_{abd}\frac{W_a}{\Omega_2-(\omega_{bd}-\omega_1+\omega_2)+i(\gamma_{bd}+\hat{\Gamma}_{bd})}\frac{1}{\Omega_1-(\omega_{ad}-\omega_1)+i(\gamma_{ad}+\hat{\Gamma}_{ad})} \quad \text{(C7)}$$

These show that $P_{\mathrm{I}}(\Omega_2, \Omega_1) + P_{\mathrm{II}}(\Omega_2, \Omega_2 - \Omega_1)$ leads to the form in eq 28 for the excited-state signal, showing a DIR.

2. Slow Bath ($\kappa \ll 1$). *Case 1*. When the input pulses are time coincident we have from eqs 29 and A1−A4

$$P_{ca}(\mathbf{k}_1-\mathbf{k}_2,t_2,0)=\exp(i(\omega_1-\omega_2)t_2)2Re\left[\left(\frac{i}{\hbar}\right)^2\sum_{abc}\mu_{ca}\mu_{bd}\mu_{ab}W_a\exp\left(-i\omega_{ca}t_2-\gamma_{ca}t_2-\frac{{\Delta_{ca}}^2{t_2}^2}{2}\right)\right] \quad \text{(C8)}$$

$$P_{bd}(\mathbf{k}_1-\mathbf{k}_2,t_2,0)=-\exp(i(\omega_1-\omega_2)t_2)2Re\left[\left(\frac{i}{\hbar}\right)^2\sum_{abd}\mu_{ad}\mu_{bd}\mu_{ba}W_a\exp\left(-i\omega_{bd}t_2-\gamma_{bd}t_2-\frac{{\Delta_{db}}^2{t_2}^2}{2}\right)\right] \quad \text{(C9)}$$

$$P_{\mathrm{II}}(t_2,0)=P_{\mathrm{I}}^*(t_2,0) \quad \text{(C10)}$$

Case 2. For well separated pulses eqs 32, 30, and A1−A4 lead to

$$P_{ca}(\mathbf{k}_1-\mathbf{k}_2,\Omega_2,\Omega_1)=\left(\frac{i}{\hbar}\right)^2\sum_{abc}\int_{-\infty}^{\infty}d\omega'\int_{-\infty}^{\infty}d\omega''\,I_{ca}(\Omega_2+\omega_1-\omega_2-\omega')\times I_{ba}(\Omega_1+\omega_1-\omega'')W_aG_1(\omega',\omega'') \quad \text{(C11)}$$

$$P_{ca}(\mathbf{k}_2-\mathbf{k}_1,\Omega_2,\Omega_1)=\left(\frac{i}{\hbar}\right)^2\sum_{abc}\int_{-\infty}^{\infty}d\omega'\int_{-\infty}^{\infty}d\omega''\,I_{ca}(\Omega_2+\omega_1-\omega_2-\omega')\times I_{cb}(\Omega_1+\omega_1-\omega'')W_cG_1(\omega',\omega'') \quad \text{(C12)}$$

$$P_{bd}(k_1-k_2,\Omega_2,\Omega_1)=-\left(\frac{i}{\hbar}\right)^2\sum_{abd}\int_{-\infty}^{\infty}d\omega'\int_{-\infty}^{\infty}d\omega''\,I_{bd}(\Omega_2+\omega_1-\omega_2-\omega')\times I_{ba}(\Omega_1+\omega_1-\omega'')W_aG_2(\omega',\omega'') \quad \text{(C13)}$$

$$P_{bd}(\mathbf{k}_2-\mathbf{k}_1,\Omega_2,\Omega_1)=-\left(\frac{i}{\hbar}\right)^2\sum_{abd}\int_{-\infty}^{\infty}d\omega'\int_{-\infty}^{\infty}d\omega''\,I_{bd}(\Omega_2+\omega_1-\omega_2-\omega')\times I_{ad}(\Omega_1+\omega_1-\omega'')W_aG_2(\omega',\omega'') \quad \text{(C14)}$$

References and Notes

(1) Andrews, D. L. *J. Phys. B* **1980**, *13*, 4091−4099.
(2) Andrews, D. L.; Allcock, P.; Demidov, A. A. *Chem. Phys.* **1995**, *190*, 1−9.
(3) Heinz, T. F. In *Nonlinear Surface Electromagnetic Phenomena*; Ponath, H. E., Stegeman, G. I., Eds.; North-Holland: Amsterdam, 1991; pp 353−416.
(4) Shen, Y. R. In *Frontiers in Laser Spectroscopy, Proceedings of the International School of Physics "Enrico Fermi", Course CXX*; Hansch, T., Inguscio, M., Eds.; North-Holland: Amsterdam, 1994; pp 139−165.
(5) Shen, Y. R. *Proc. Natl. Acad. Sci.* **1996**, *93*, 12104−12111.
(6) Richmond, G. L. *Annu. Rev. Phys. Chem.* **2001**, *52*, 357−389.
(7) Moad, A. J.; Simpson, G. J. *J. Phys. Chem. B* **2004**, *108*, 3548−3562.
(8) Guyot-Sionnest, P.; Dumas, P.; Chabal, Y. *J. Elec. Spec. Relat. Phenom.* **1990**, *54/55*, 27−38.
(9) Ueba, H. *Prog. Surf. Sci.* **1997**, *55*, 115−179.
(10) Bonvalet, A.; Nagle, J.; Berger, V.; Migus, A.; Martin, J.-L.; Joffre, M. *Phys. Rev. Lett.* **1996**, *76* (23), 4392−4395.
(11) Belabas, N.; Joffre, M. *Opt. Lett.* **2002**, *27* (22), 2043−2045.
(12) Masahito, O.-e.; Lvovsky, A. I.; Wei, X.; Shen, Y. R. *J. Chem. Phys.* **2000**, *113* (19), 8827−8832.
(13) Belkin, M. A.; Shen, Y. R. *Phys. Rev. Lett.* **2003**, *91* (21), 213907/1−213907/4.
(14) Burke, B. J.; Moad, A. J.; Polizzi, M. A.; Simpson, G. J. *J. Am. Chem. Soc.* **2003**, *125*, 9111−9115.
(15) Koroteev, N. I.; Makarov, V. A.; Volkov, S. N. *Opt. Comm.* **1998**, *157*, 111−114.
(16) Morita, A.; Hynes, J. T. *J. Phys. Chem. B* **2002**, *106* (3), 673−685.
(17) Perry, A.; Ahlborn, H.; Space, B.; Moore, P. B. *J. Chem. Phys.* **2003**, *118* (18), 8411−8419.
(18) Yeh, Y. L.; Zhang, C.; Held, H.; Mebel, A. M.; Wei, X.; Lin, S. H.; Shen, Y. R. *J. Chem. Phys.* **2001**, *114* (4), 1837−1843.
(19) Groot, M. L.; Vos, M. H.; Schlichting, I.; van Mourik, F.; Joffre, M.; Lambry, J. C.; Martin, J. L. *Proc. Natl. Acad. Sci.* **2002**, *99*, 1323−1328.
(20) Groma, G. I.; Colonna, A.; Lambry, J. C.; Petrich, J. W.; Varo, G.; Joffre, M.; Vos, M. H.; Martin, J. L. *Proc. Natl. Acad. Sci.* **2004**, *101*, 7971−7975.
(21) Mukamel, S. *Principles of nonlinear optical spectroscopy*; Oxford University Press: New York, 1995.
(22) Hayashi, M.; Lin, S. H.; Raschke, M. B.; Shen, Y. R. *J. Phys. Chem. A* **2002**, *106* (10), 2271−2282.
(23) Prior, Y.; Bogdan, A. R.; Dagenais, M.; Bloembergen, N. *Phys. Rev. Lett.* **1981**, *46* (2), 111−114.
(24) Andrews, J. R.; Hochstrasser, R. M. *Chem. Phys. Lett.* **1981**, *83* (3), 427−431.
(25) Dick, B.; Hochstrasser, R. M. *Phys. Rev. Lett.* **1983**, *51* (24), 2221−2223.
(26) Chang, T. C.; Johnson, C. K.; Small, G. J. *J. Phys. Chem.* **1985**, *89*, 2984−2992.
(27) Wright, J. C.; Condon, N. J.; Murdoch, K. M.; Besemann, D. M.; Meyer, K. A. *J. Phys. Chem. A* **2003**, *107* (18), 8166−8176.
(28) Mukamel, S. *Phys. Rev. A* **1983**, *28* (6), 3480−3492.
(29) Sue, J.; Yan, Y.; Mukamel, S. *J. Chem. Phys.* **1986**, *85*, 462−474.